

**Contribution of L-type Ca<sup>2+</sup> channels to early afterdepolarizations induced by I<sub>Kr</sub> and I<sub>Ks</sub> channel suppression in guinea-pig ventricular myocytes**

Authors:

Mitsuhiko Yamada\*, Keisuke Ohta, Atsunori Niwa, Natsuko Tsujino, Tsutomu Nakada and Masamichi Hirose

Department of Molecular Pharmacology, Shinshu University School of Medicine

\*Corresponding Author:

Mitsuhiko Yamada, M.D., Ph.D.

Department of Molecular Pharmacology, Shinshu University School of Medicine

3-1-1 Asahi, Matsumoto, Nagano

390-8621

Japan

E-mail: myamada@sch.md.shinshu-u.ac.jp

Phone: +81-263-37-2605

Fax: +81-263-37-3085

## Abstract

Early afterdepolarizations (EADs) induced by suppression of cardiac delayed rectifier  $I_{Kr}$  and/or  $I_{Ks}$  channels cause fatal ventricular tachyarrhythmias. In guinea-pig ventricular myocytes, partial block of one of the channels with complete block of the other reproducibly induced EADs. Complete block of both  $I_{Kr}$  and  $I_{Ks}$  channels depolarized the take-off potential and reduced the amplitude of EADs, which in some cases were not clearly separated from the preceding action potentials. A selective L-type  $Ca^{2+}$  ( $I_{Ca,L}$ ) channel blocker, nifedipine, effectively suppressed EADs at submicromolar concentrations. As examined with the action potential-clamp method,  $I_{Ca,L}$  channels mediated inward currents with a spike and dome shape during action potentials.  $I_{Ca,L}$  currents decayed mainly due to inactivation in phase 2 and deactivation in phase 3 repolarization. When EADs were induced by complete block of  $I_{Kr}$  channels with partial block of  $I_{Ks}$  channels, repolarization of the action potential prior to EAD take-off failed to increase  $I_{K1}$  currents and thus failed to completely deactivate  $I_{Ca,L}$  channels which reactivated and mediated inward currents during EADs. When both  $I_{Kr}$  and  $I_{Ks}$  channels were completely blocked,  $I_{Ca,L}$  channels were not deactivated and mediated sustained inward currents until the end of EADs. Under this condition, the recovery and reactivation of  $I_{Ca,L}$  channels were absent before EADs. Therefore, an essential mechanism underlying EADs caused by suppression of the delayed rectifiers is the failure to completely deactivate  $I_{Ca,L}$  channels.

## **Key Words**

Early afterdepolarizations,  $I_{Kr}$  channels,  $I_{Ks}$  channels, L-type  $Ca^{2+}$  channels, Long QT syndrome, Action potential clamp, Cardiac electrophysiology

## Introduction

The voltage-dependent L-type  $\text{Ca}^{2+}$  ( $I_{\text{Ca,L}}$ ) channel is the main source of  $\text{Ca}^{2+}$  entry during an action potential in cardiac myocytes (McDonald et al., 1994). During an action potential, an  $I_{\text{Ca,L}}$  current shows the form of a spike followed by a dome (Doerr et al., 1990; Arreola et al., 1991; Grantham & Cannel, 1996; Linz and Myer, 1998a & 2000). The initial spike causes  $\text{Ca}^{2+}$  release from the sarcoplasmic reticulum whereas the following slow dome component re-loads the sarcoplasmic reticulum (Fabiato, 1985; Linz and Myer, 1998b). The form of  $I_{\text{Ca,L}}$  currents during action potentials is finely tuned by inactivation, deactivation and alterations in the driving force (Luo & Rudy, 1994; Linz and Myer, 1998a). Inactivation of cardiac  $I_{\text{Ca,L}}$  channels is both voltage- and  $\text{Ca}^{2+}$ -dependent (Kass & Sanguinetti, 1984; Lee et al., 1985). Impairment of either type of inactivation results in prominent prolongation of cardiac action potentials (Alseikhan et al., 2002; Splawski et al., 2004), indicating that  $I_{\text{Ca,L}}$  channels play a significant role in determining cardiac action potential duration.

Long QT (LQT) syndrome describes a group of disorders that is usually characterized by a prolonged QT interval on the electrocardiogram (Keating & Sanguinetti, 2001). It is associated with syncope and sudden death due to episodic cardiac arrhythmias. Among the 8 types of congenital LQT syndrome, LQT1 is the most frequent and caused by impairment of the slow component of delayed rectifier  $\text{K}^+$  current ( $I_{\text{Ks}}$ ). A more common acquired LQT syndrome can arise from suppression of the rapid component of delayed rectifier  $\text{K}^+$  current ( $I_{\text{Kr}}$ ) by various factors including drugs.

In LQT syndromes, the action potentials of ventricular myocytes are prolonged and may be associated with early afterdepolarizations (EADs). EADs are defined as depolarizing afterpotentials that interrupt or delay normal repolarization of cardiac action potentials (Cranefield & Aronson, 1988). Depending on the membrane potential at which EADs take off, they are classified into two categories: low-membrane potential (or phase 2) EADs that occur during phase 2 repolarization, and high-membrane potential (or phase 3) EADs that occur during phase 3 repolarization (Damiano & Rose, 1984). The former arise from the reduction of net outward currents during phase 2 repolarization which occurs in LQT syndromes (Brugada & Wellens, 1985; Antzelevitch & Shimizu, 2002; Splawski et al., 2004).

It has been suggested that when delayed rectifier  $\text{K}^+$  currents are reduced an  $I_{\text{Ca,L}}$  channel causes the phase 2 EADs (Marbán et al., 1986; Anderson et al., 1998; Zeng & Rudy, 1995). January and Riddle (1989) found that the  $I_{\text{Ca,L}}$  channel agonist BayK8644 caused EADs taking off at  $\sim -30$  mV and having an amplitude of up to  $\sim 40$  mV in sheep

Purkinje fibers and concluded that  $I_{Ca,L}$  channels recovered before EADs and generated EADs. This mechanism is also suggested to underlie EADs caused by suppression of  $K^+$  currents by a theoretical study (Zeng & Rudy, 1995). However, this notion has not been experimentally tested.

In this study of isolated guinea-pig ventricular myocytes we found that when  $I_{Kr}$  and  $I_{Ks}$  channels were suppressed, EADs took off from a more depolarized potential ( $\sim -10$  mV) and had a much smaller amplitude ( $< 15$  mV) than January and Riddle (1989) found. Under this condition, the recovery of  $I_{Ca,L}$  channels before EADs was modest if any, and EADs arose mainly from the failure to deactivate  $I_{Ca,L}$  channels and the resulting sustained inward current at the end of phase 2 repolarization.

## Methods

### Isolation of cardiac myocytes

Ventricular myocytes were enzymatically isolated from the hearts of male guinea-pigs (300-600 g) as previously described (Yamada et al., 1993). Briefly, the animals were killed with intraperitoneal injection of 50-200 mg of pentobarbital. The hearts were quickly removed and retrogradely perfused in a Langendorff apparatus with 400 mL of modified Tyrode solution (for composition, see below) and then with 100 mL of nominally  $\text{Ca}^{2+}$ -free Tyrode solution (for composition, see below) at 37 °C. Thereafter, the hearts were digested with nominally  $\text{Ca}^{2+}$ -free Tyrode solution containing 0.3 mg/mL collagenase at 37 °C for 55 min. The reaction was terminated with perfusion of 50 mL KB solution (for composition, see below). The digested hearts were stored in KB solution at 4 °C for up to 6 hr before use. Ventricular myocytes were isolated by gently shaking a small piece of the ventricular myocardium in a recording chamber filled with the modified Tyrode solution. All experiments were carried out in accordance with the Guidelines for Animal Experimentation of Shinshu University.

### Electrophysiology

Membrane voltage and currents were recorded with a patch-clamp amplifier (Axopatch 200B, Molecular Devices Corp., Sunnyvale, CA, USA) in the whole-cell configuration of the patch-clamp method (Hamill et al., 1981). In all experiments, data acquisition was done with an in-house computer program. Patch pipettes were fabricated from borosilicate glass capillaries (Kimax-51, Kimble Glass Inc., Vineland, NJ, USA) and had a resistance of  $\leq 2 \text{ M}\Omega$  when filled with pipette solution (for composition, see below). The pipette offset potential, series resistance, and cell capacitance were compensated with the amplifier. The series resistance and membrane capacitance compensation was repeatedly adjusted every 2-3 minutes during experiments and were  $3.7 \pm 0.1 \text{ M}\Omega$  and  $170.7 \pm 4.1 \text{ pF}$  at the end of experiments, respectively ( $n = 239$ ). A leak current was not subtracted. All experiments were done in modified Tyrode solution at 35-37 °C unless otherwise indicated.

In current-clamp experiments, action potentials were elicited with a rectangular current pulse of 1-4 nA and 2 msec duration at 0.33 Hz. Recorded action potentials were low-pass filtered at 2 kHz (-3 dB), digitized at 5 kHz and stored on a hard disk of a computer. In some experiments, E4031, chromanol 293B (293B), nifedipine and/or SEA0400 were used to block respectively  $I_{\text{Kr}}$ ,  $I_{\text{Ks}}$ ,  $I_{\text{Ca,L}}$  channels and  $\text{Na}^+$ - $\text{Ca}^{2+}$  exchange.

It has been reported that there are M cells in the guinea-pig ventricle (Sicouri et al., 1996). Compared with other ventricular myocytes, M cells show a disproportionate

prolongation of their action potentials in response to either slowing of the stimulation rate or the application of class III antiarrhythmic drugs. In our hands, however, it was difficult to reliably and reproducibly isolate M cells from the digested whole ventricle. In addition, we did not find any cells where E4031 (10  $\mu$ M) alone significantly prolonged action potential duration or caused EADs (Fig. 1). Thus, we did not distinguish M cells from other myocardial cells in this study.

Action potential-clamp experiments were conducted following the protocols outlined by Linz & Meyer (1998a). Four action potentials representing different experimental conditions were recorded under current-clamp, DA converted and subsequently used as voltage command pulses (Figs. 3-6). Each action potential stimulus was preceded by a 200 msec rectangular pulse to -40 mV to inactivate voltage-dependent Na<sup>+</sup> channels and T-type Ca<sup>2+</sup> channels (Linz & Myer, 1998a). The holding potential was -80 mV. Each action potential stimulus was applied to myocytes at 0.33 Hz.

An I<sub>Ca,L</sub> current was isolated as the membrane current that was inhibited by the addition of 100  $\mu$ M Cd<sup>2+</sup> and 10  $\mu$ M nifedipine. Nifedipine (10  $\mu$ M) alone did not completely suppress the initial part of I<sub>Ca,L</sub> currents while Cd<sup>2+</sup> (100  $\mu$ M) failed to completely suppress the late phase of I<sub>Ca,L</sub> currents in action potentials. I<sub>Kr</sub> and I<sub>Ks</sub> currents were respectively isolated as E4031 (10  $\mu$ M) or 293B (50  $\mu$ M) sensitive difference currents. An I<sub>K1</sub> current was isolated as the Ba<sup>2+</sup> (2 mM) sensitive difference current. To isolate each membrane current during action potential stimuli, these drugs were added sequentially in this order in a cumulative manner.

The steady-state activation of I<sub>Ca,L</sub> channels ( $d_{\infty}$ ) was estimated with conventional rectangular voltage-clamp steps. In these experiments, the membrane potential was depolarized from -80 mV to -40 mV for 200 msec and then for 500 msec to potentials between -40 and +70 mV with a 5 mV increment every 3 sec. The peak amplitude of I<sub>Ca,L</sub> currents evoked by the 500 ms test pulse was normalized to the membrane capacitance and plotted against membrane voltage. The peak current density-voltage relationship was fitted with the following equation.

$$I = g_{Ca,L} (I / (1 + \text{Exp} ((V_{0.5} - V_m) / k))) (V_m - E_{Ca}), \quad \text{Eq. 1}$$

where  $I$  is the peak I<sub>Ca,L</sub> density;  $g_{Ca,L}$ , the maximum conductance density of I<sub>Ca,L</sub> channels;  $V_{0.5}$ , the membrane potential at which  $d_{\infty} = 0.5$ ;  $V_m$ , the membrane potential;  $k$ , the slope factor; and  $E_{Ca}$ , the apparent reversal potential of I<sub>Ca,L</sub> channels. The best fit of this equation to the data was obtained with  $g_{Ca,L}$  181 pS/pF,  $V_{0.5}$  -13.9 mV,  $k$  5.13 mV and  $E_{Ca}$  +57.8 mV. From these parameters,  $d_{\infty}$  was calculated from the following

equation.

$$d_{\infty} = I / (I + \text{Exp}((V_{0.5} - V_m) / k)) \quad \text{Eq. 2}$$

Then, the activation of  $I_{Ca,L}$  channels during action potentials ( $d_{AP}$ ) was calculated from equation 2 and the time-dependent change in  $V_m$ , except for the initial 4 msec. This assumes that the activation kinetics of  $I_{Ca,L}$  channels are sufficiently fast compared with the time-dependent change in  $V_m$  (Linz & Myer, 2000).

Inactivation of  $I_{Ca,L}$  channels during action potentials ( $f_{AP}$ ) was assessed with a gapped double pulse protocol (Linz & Myer, 1998a). In this protocol, the membrane potential was first depolarized from the resting membrane potential (~-80 mV) to -40 mV for 200 msec and then an action potential wave form was applied (P1). The action potential was interrupted at different times and voltage values with a voltage step to -40 mV for 5 msec followed by a 200 ms test pulse to +10 mV (P2).  $f_{AP}$  was assessed by normalizing the amplitude of  $I_{Ca,L}$  currents during P2 in the presence of P1 relative to that which had been recorded in the absence of P1.

Inactivation of  $I_{Ca,L}$  channels is both voltage- and  $Ca^{2+}$ -dependent (Kass & Sanguinetti, 1984; Lee et al., 1985). Total  $f_{AP}$  was assessed as above in solution containing 1.8 mM  $Ca^{2+}$ . The voltage-dependent component of inactivation in action potentials ( $f_{AP\_V}$ ) was assessed in solution containing 1.8 mM  $Ba^{2+}$  instead of  $Ca^{2+}$  (Kass & Sanguinetti, 1984; Lee et al., 1985). The  $Ca^{2+}$ -dependent component of inactivation in action potentials ( $f_{AP\_Ca}$ ) was calculated with equation 3 assuming that voltage- and  $Ca^{2+}$ -dependent inactivation occur through independent mechanisms (Hardley & Lederer, 1991; Linz & Myer, 1998a; Shirokov et al., 1993).

$$f_{AP} = f_{AP\_V} f_{AP\_Ca} \quad \text{Eq. 3}$$

### Data Analysis

Recorded cell currents were low-pass filtered at 10 kHz (-3 dB), digitized at 47.2 kHz with a PCM converter system (VR-10B, Instrutech Corp., New York, NY, USA) and recorded on videocassette tapes. For off-line analysis, data were reproduced, low-pass filtered at 2 kHz (-3 dB), digitized at 5 kHz with an AD converter (ITC161, Instrutech Corp., New York, NY, USA) and analyzed with Patch Analyst Pro (MT Corp., Hyogo, Japan).

### Solutions and Chemicals

The modified Tyrode solution contained (in mM): 136.5 NaCl, 5.4 KCl, 1.8  $CaCl_2$ ,

0.53 MgCl<sub>2</sub>, 5.5 glucose and 5.5 HEPES (pH adjusted to 7.4 with NaOH). CaCl<sub>2</sub> was omitted for the nominally Ca<sup>2+</sup>-free Tyrode solution. In some experiments 1.8 mM BaCl<sub>2</sub> replaced 1.8 mM CaCl<sub>2</sub>. The KB solution contained (in mM): 10 taurine, 10 oxalic acid, 70 L-glutamic acid, 25 KCl, 10 KH<sub>2</sub>PO<sub>4</sub>, 11 glucose, 0.5 EGTA and 10 HEPES (pH was adjusted 7.3 with KOH). The pipette solution contained (in mM): 120 potassium D-glutamate, 20 KCl, 10 NaCl, 5 MgCl<sub>2</sub>, 0.1 EGTA, 3 ATP and 5 HEPES (pH was adjusted to 7.4 with KOH). Stock solutions of nifedipine, 293B and SEA0400 were prepared in 100 % DMSO at 10, 50 and 10 mM, respectively. Final dilutions were in the modified Tyrode solution. The maximum final concentration of DMSO (0.1 %) did not affect membrane currents.

SEA0400 was provided by Taisho Pharmaceutical Co. Ltd. (Tokyo, Japan). Pentobarbital sodium was purchased from Abott Laboratories (North Chicago, IL, USA). Collagenase was from Worthington Biochemical (Type II, Freehold, NJ, USA). Nifedipine and E4031 were from Wako Pure Chemical Industries, Ltd. (Osaka, Osaka, Japan). 293B was from Sigma-Aldrich, Inc. (St. Lois, MO, USA). All other chemicals were purchased from Wako Pure Chemical Industries , Ltd.

### **Statistical Analysis**

Data values are shown as mean ± SE. Statistical differences were evaluated with Student's paired or unpaired t-test. A value of P<0.05 was considered significant.

## Results

### Early afterdepolarizations can be induced by $I_{Kr}$ and $I_{Ks}$ blockers

Figure 1 shows the induction of EADs in action potentials by blockade of different  $K^+$  currents. Action potentials were induced by pacing isolated myocytes at 0.33 Hz in the presence or absence of different concentrations of the  $I_{Kr}$  blocker E4031 and the  $I_{Ks}$  blocker chromanol 293B (293B) (Sanguinetti & Jurkiewicz, 1990; Bosch et al., 1998). This pacing frequency was chosen since EADs tend to occur at bradycardia (Cranefield & Aronson, 1988). Compared with the control (Fig. 1A), 10  $\mu$ M E4031 alone only slightly prolonged action potential duration and did not induce EADs (Fig. 1B). The further addition of 20  $\mu$ M 293B strongly prolonged action potential duration and induced EADs (Fig. 1C). EADs arose when action potential repolarization reached -8-0 mV, they were sustained for as long as ~2 sec and they had an amplitude of 2-15 mV. When the concentration of 293B was increased to 50  $\mu$ M, a diminished amplitude (~2 mV) of EADs occurred from a more depolarized take-off potential (~0 mV) (Fig. 1D). Similar results were obtained in nine other myocytes.

In another myocyte, 50  $\mu$ M 293B alone only slightly prolonged action potential duration (Fig. 1F) compared with control (Fig. 1E). However, the addition of 100 nM E4031 significantly prolonged action potential duration and induced EADs (Fig. 1G). Here EADs arose when action potential repolarization reached ~-4-0 mV, they were sustained for 1-2 sec and they had an amplitude of 2-3 mV. Increasing the concentration of E4031 to 1  $\mu$ M even further prolonged action potential duration and induced EADs which were sustained for more than 2.5 sec (Fig. 1H). Similar results were obtained in nine other myocytes.

Thus, the blockade of either  $I_{Kr}$  or  $I_{Ks}$  channels alone was not sufficient to prolong action potential duration or induce EADs in isolated guinea-pig ventricular myocytes. But the partial blockade of one in the presence of complete blockade of the other strongly prolonged action potential duration and induced EADs. Complete blockade of both  $I_{Kr}$  and  $I_{Ks}$  channels depolarized the take-off potential and diminished the amplitude of EADs, which in some cases could not be clearly separated from the preceding action potential (more clearly represented in Figs. 5A and 5B). We regarded this type EADs and the prototypical EADs with a clear take-off and depolarization as a continuous spectrum because the latter was gradually transformed to the former as the blockade of  $I_{Kr}$  and  $I_{Ks}$  channels was progressively strengthened. EADs fused with action potentials did not seem to arise from rundown of inward currents generating EADs because this type of EADs also appeared when 10  $\mu$ M E4031 and 50  $\mu$ M 293B were applied soon after formation of the whole-cell configuration (see Fig. 2A).

### **Effect of nifedipine on early afterdepolarizations**

The upper panel in Figure 2A shows the effect of nifedipine (10 and 100 nM) on action potentials without EADs under control conditions. Action potentials were elicited by pacing a myocyte at 0.33 Hz. Nifedipine reduced APD<sub>90</sub> from 448 to 417 (10 nM) and 320 (100nM) msec. The lower panel in Figure 2A shows the effect of nifedipine on action potentials with EADs. Action potentials were elicited by pacing a myocyte at 0.33 Hz in the presence of 10  $\mu$ M E4031 and 50  $\mu$ M 293B. Nifedipine reduced the duration for 90 % repolarization from 1,653 to 1,188 (10 nM) and 591 (100 nM) msec.

Figure 2B shows that nifedipine reduced APD<sub>90</sub> more potently in the presence of E4031 and 293B than under control conditions. These results indicate that I<sub>Ca,L</sub> channels may play a more important role in determining the time course of repolarization of action potentials with EADs than those without EADs and therefore I<sub>Ca,L</sub> channels could be critically involved in the genesis and maintenance of EADs.

It has been suggested that Na<sup>+</sup>-Ca<sup>2+</sup> exchanger (I<sub>Na-Ca</sub>) currents also participate in genesis of EADs (Priori & Corr, 1990; Nagy et al., 2004). Thus, we examined the effect of a selective I<sub>Na-Ca</sub> blocker, SEA0400 on EADs elicited by 10  $\mu$ M E4031 and 50  $\mu$ M 293B. SEA0400 blocks I<sub>Na-Ca</sub> with a half-maximum inhibitory concentration of 5-100 nM (Matsuda et al., 2001; Birinyi et al., 2005). SEA0400 reduced APD<sub>90</sub> to 90.4  $\pm$  4.1 % (100 nM) and 85.7  $\pm$  6.0 % (1  $\mu$ M) of the control (not shown) (n = 5 for each concentration). These effects were much smaller than those of nifedipine (Fig. 2B). Thus, I<sub>Ca,L</sub> channels seem likely to play a more important role than I<sub>Na-Ca</sub> in the genesis of EADs when I<sub>Kr</sub> and I<sub>Ks</sub> channels are blocked (Zeng & Rudy, 1995).

### **L-type Ca<sup>2+</sup> and K<sup>+</sup> currents recorded during guinea-pig ventricular action potentials**

We therefore examined the behavior of I<sub>Ca,L</sub> channels during action potentials. Figure 3 shows total membrane, I<sub>Ca,L</sub> and K<sup>+</sup> channel currents measured in action potential-clamp experiments. Two different action potential stimuli were used in this analysis (Figs. 3A and 3B). These action potentials were originally recorded from two different myocytes which had been paced at 0.33 Hz. The action potential in A was recorded under control conditions and that shown in B was recorded in the presence of 10  $\mu$ M E4031 and 10  $\mu$ M 293B. In the following experiments, each action potential stimulus was applied to isolated myocytes at 0.33 Hz.

Figures 3C and 3D show the total membrane currents evoked during each action potential. They were outward, increasing gradually during phase 2 repolarization and then rapidly and transiently increased during phase 3 repolarization. The gray trace in

Figure 3D shows that the total membrane current in the presence of 10  $\mu\text{M}$  E4031 and 10  $\mu\text{M}$  293B was reduced by comparison with the current recorded in control solution (black trace).

An  $I_{\text{Ca,L}}$  current was isolated as that part of the total membrane current that was inhibited by 100  $\mu\text{M}$   $\text{Cd}^{2+}$  and 10  $\mu\text{M}$  nifedipine. In each action potential, an  $I_{\text{Ca,L}}$  current was always inward with a spike and dome shape (Figs. 3E and 3F). The peak  $I_{\text{Ca,L}}$  densities were  $-3.02 \pm 1.43$  (E) and  $-2.14 \pm 0.53$  (F) pA/pF.

$I_{\text{Kr}}$  and  $I_{\text{Ks}}$  currents were respectively isolated as the 10  $\mu\text{M}$  E4031 and 50  $\mu\text{M}$  293B sensitive parts of the membrane current. Outward  $I_{\text{Kr}}$  currents gradually increased during phase 2 and rapidly decreased in phase 3 of the action potential (Fig. 3G). The  $I_{\text{Kr}}$  density reached a peak of  $0.89 \pm 0.07$  pA/pF at -29 mV (G). The black trace in Figure 3H illustrates  $I_{\text{Kr}}$  currents recorded in control solution which should have been absent when the action potential (B) was recorded in the presence of 10  $\mu\text{M}$  E4031.

$I_{\text{Ks}}$  currents initially increased then decreased gradually during phase 2 repolarization (Figs. 3I and 3J). It decreased rapidly during phase 3. The gray trace in Figure 3J illustrates the extent of  $I_{\text{Ks}}$  inhibition by 10  $\mu\text{M}$  293B compared to that recorded in control solution (black).

Figures 3K and 3L show that inward-rectifier  $I_{\text{K1}}$  currents was small and outward during phase 2 repolarization of each action potential. In phase 3 repolarization  $I_{\text{K1}}$  currents first abruptly increased and then decreased as the membrane voltage approached the resting value.

### **The kinetics of L-type $\text{Ca}^{2+}$ channels during action potential clamp**

$I_{\text{Ca,L}}$  currents in cardiac action potentials can be described in the following extended Hodgkin-Huxley equation (Luo & Rudy, 1994; Linz & Myer, 1998a & 2000):

$$I_{\text{Ca,L}} = g_{\text{Ca,L}} d_{\text{AP}} f_{\text{AP}} (V_m - E_{\text{Ca}}), \quad \text{Eq. 4}$$

where  $I_{\text{Ca,L}}$  is  $I_{\text{CaL}}$  currents in an action potential.

The characteristics of activation ( $d_{\text{AP}}$ ) and inactivation ( $f_{\text{AP}}$ ) of  $I_{\text{CaL}}$  channels during the two different action potential waveforms were dissected.  $f_{\text{AP}}$  was assessed with the gapped action potential clamp technique (Linz & Myer, 1998a). Figures 4A and 4B illustrate the uninterrupted action potentials. Figures 4C and 4D illustrate the time-dependent changes in  $d_{\text{AP}}$ ,  $f_{\text{AP}}$  and  $f_{\text{AP}_V}$  during each action potential. In each action potential,  $d_{\text{AP}}$  was almost unity during the peak and phase 2 repolarization and decreased rapidly to zero during phase 3 repolarization. Thus,  $I_{\text{Ca,L}}$  channels show deactivation during phase 3 repolarization.

The time-dependent change in  $f_{AP}$  was measured with 1.8 mM  $\text{Ca}^{2+}$  in the external solution. In each action potential  $f_{AP}$  gradually decreased during phase 2 and increased during phase 3 repolarization (Figs. 4C and 4D). The time at which  $f_{AP}$  was minimal ( $T_{min}$ ) was 368 (C) and 506 (D) msec. At  $T_{min}$ ,  $f_{AP}$  was 0.085 (C) and 0.071 (D). Thus,  $\text{I}_{\text{Ca,L}}$  channels were not completely inactivated and they showed partial recovery during each action potential (Luo & Rudy, 1994; Linz & Myer, 1998a & 2000).

The voltage-dependent inactivation of  $\text{I}_{\text{Ca,L}}$  channels in action potentials was assessed in the presence of 1.8 mM  $\text{Ba}^{2+}$  ( $f_{AP_V}$  in Figs. 4C and 4D). Although the values for  $f_{AP_V}$  were larger than  $f_{AP}$  throughout each action potential, it also decreased during phase 2 and increased during phase 3.  $f_{AP_V}$  minima were 0.430 at 368 msec (C) and 0.301 at 577 msec (D).

From  $f_{AP}$  and  $f_{AP_V}$ , the  $\text{Ca}^{2+}$ -dependent component of inactivation of  $\text{I}_{\text{Ca,L}}$  channels in action potentials ( $f_{AP_{Ca}}$ ), a fraction of  $f_{AP}$ , was calculated with Eq. 3 (Figs. 4E and 4F). In each action potential,  $f_{AP_{Ca}}$  first rapidly and then more gradually decreased during phase 2 repolarization before increasing during phase 3.  $f_{AP_{Ca}}$  minima were 0.198 at 368 msec (E) and 0.220 at 506 msec (H). Values for  $f_{AP_{Ca}}$  were smaller than  $f_{AP_V}$  throughout phase 2 of each action potential.

These results suggest that  $\text{Ca}^{2+}$ -dependent inactivation plays a more important role than voltage-dependent inactivation during the first 10 msec and this is responsible for the initial rapid decay of  $\text{I}_{\text{Ca,L}}$  currents during the action potentials (Figs. 3E and 3F). This rapid inactivation may mainly result from the release of  $\text{Ca}^{2+}$  from sarcoplasmic reticulum (Linz & Myer, 1998a). Subsequently during phase 2 repolarization, both voltage- and  $\text{Ca}^{2+}$ -dependent inactivation almost equally contributed to the decay of  $\text{I}_{\text{Ca,L}}$  currents. But,  $\text{I}_{\text{Ca,L}}$  channels were incompletely inactivated at  $T_{min}$  and then showed recovery. Thus, the decay of  $\text{I}_{\text{Ca,L}}$  currents after  $T_{min}$  was due to deactivation (Luo & Rudy, 1994; Linz & Myer, 1998a & 2000).

### **$\text{K}^+$ currents responsible for deactivation of L-type $\text{Ca}^{2+}$ channels during the action potential**

At  $T_{min}$   $\text{I}_{\text{Ca,L}}$  channels still mediate substantial inward currents because although  $f_{AP}$  is small,  $d_{AP}$  and  $(V_m - E_{Ca})$  are large (Eq. 4, Figs. 3E, 3F, 4C and 4D). The  $\text{I}_{\text{Ca,L}}$  currents remaining at  $T_{min}$  must be eliminated by deactivation for which repolarizing  $\text{K}^+$  currents should be responsible. The left column of data in Figure 3 shows that  $\text{I}_{\text{Kr}}$ ,  $\text{I}_{\text{Ks}}$ , and  $\text{I}_{\text{K1}}$  channels mediate such currents. In particular  $\text{I}_{\text{K1}}$  channels were activated soon after  $T_{min}$  and mediated very large outward currents (Fig. 3K). Thus, it is likely that activation of  $\text{I}_{\text{Kr}}$  and  $\text{I}_{\text{Ks}}$  channels during phase 2 repolarization lead to regenerative activation of  $\text{I}_{\text{K1}}$  channels and thereby complete deactivation of  $\text{I}_{\text{Ca,L}}$  channels during phase 3

repolarization.

However, when  $I_{Kr}$  and  $I_{Ks}$  channels were blocked (right column in Fig. 3), the repolarization rate around  $T_{min}$  was diminished ( $dV/dt$  at  $T_{min}$  was -0.78 (A) and -0.16 (B) V/sec), and  $I_{K1}$  currents now increased ~50 msec after  $T_{min}$  (Fig. 3L). This delayed increase in  $I_{K1}$  currents delayed deactivation of  $I_{Ca,L}$  channels (Fig. 4D) and  $I_{Ca,L}$  channels mediated inward currents for a longer time after  $T_{min}$  in the presence of the blockers (Fig. 3F).

### **L-type $Ca^{2+}$ and $K^+$ currents during action potentials with early afterdepolarizations**

In order to evaluate  $I_{Ca,L}$  and  $K^+$  currents during action potentials which showed EADs we used the two exemplar action potentials shown in Fig. 5 as action potential-clamp stimuli. That shown in Figure 5A was recorded from a myocyte treated with 10  $\mu$ M E4031 and 20  $\mu$ M 293B. This action potential had an EAD with a take-off potential of ~-6 mV and an amplitude of ~7 mV. That shown in Figure 5B was recorded from a different myocyte which had been treated with 10  $\mu$ M E4031 and 50  $\mu$ M 293B. In this case, EADs could not be clearly separated from the preceding action potential due to a depolarized take-off potential and a diminished amplitude.

The black traces in Figures 5C and 5D were total membrane currents recorded under the control condition while the gray indicate those in the presence of 10  $\mu$ M E4031 and 20  $\mu$ M 293B (C) or 10  $\mu$ M E4031 and 50  $\mu$ M 293B (D). In both cases, total membrane currents were outward and fluctuated before abruptly increasing and then decreasing at the end of the EADs. In the left-hand column of Fig. 5,  $I_{Ca,L}$  channels mediated an inward current throughout the action potential and the EAD (Fig. 5E).  $I_{Ca,L}$  currents did not decay smoothly but exhibited a small notch (arrow) on the upstroke of the EAD.  $I_{Kr}$  currents in Figure 5G were recorded in the control condition but should have been absent when the action potential (A) was recorded in the presence of 10  $\mu$ M E4031. The black trace in Figure I indicates an  $I_{Ks}$  current in the control condition while the gray that in the presence of 20  $\mu$ M 293B. The latter transiently increased during phase 2 of the action potential and stayed almost constant throughout the EAD.  $I_{K1}$  currents slightly increased before the EAD took off (arrow head) and abruptly increased when the EAD terminated (Fig. 5K).

In the right-hand column of Fig. 5,  $I_{Ca,L}$  channels again mediated an inward current throughout the action potential and EADs (Fig. 5F). In this case,  $I_{Ca,L}$  currents decayed smoothly and did not show discernable notches.  $I_{Kr}$  and  $I_{Ks}$  currents shown in Figures 5H and 5J were recorded under the control condition but should have been absent when the action potential B was recorded in the presence of 10  $\mu$ M E4031 and 50  $\mu$ M 293B.

$I_{K1}$  channels mediated an almost constant outward current throughout the action potential and EADs and a large transient outward current at the end of the EADs (Fig. 5L). Together these results suggest that  $I_{Ca,L}$  and  $I_{K1}$  channels play pivotal roles in the genesis and termination of EADs.

### **The kinetics of L-type $Ca^{2+}$ channels during action potentials with early afterdepolarizations**

The activation, inactivation, and recovery of  $I_{Ca,L}$  channels during action potentials with EADs are shown in Fig. 6. In the left-hand column,  $d_{AP}$  transiently decreased to 0.82 before the EAD took off and then increased to 0.95 during the upstroke of the EAD (Fig. 6C). Thereafter,  $d_{AP}$  gradually decreased before promptly declining to zero at the end of the EAD.  $f_{AP}$  decreased during phase 2 of the action potential but slightly and significantly increased just before the EAD took off (Fig. 6C). Thereafter,  $f_{AP}$  decreased to a minimum of 0.019 at 933 msec.  $f_{AP_V}$  almost monotonously decreased until the end of the EAD and it did not exhibit a clear notch before the EAD took off (Fig. 6C).  $f_{AP_{Ca}}$  decreased during the action potential and showed a small notch before the EAD took off (Fig. 6E). Thus,  $I_{Ca,L}$  channels were partially deactivated and modestly recovered from  $Ca^{2+}$ -induced inactivation as the EAD took off. In the upstroke of the EAD,  $I_{Ca,L}$  channels were reactivated and formed the notch of  $I_{Ca,L}$  currents (Fig. 5E, an arrow). At  $T_{min}$ ,  $f_{AP}$  was small (0.019) but  $I_{Ca,L}$  channels still mediated a measurable inward current because  $d_{AP}$  and the driving force were relatively large (Eq. 4, Figs. 5E and 6C). After  $T_{min}$ ,  $I_{Ca,L}$  channels mediated an inward current until it was completely deactivated by  $I_{K1}$  currents ~190 msec after  $T_{min}$  (Figs. 5E, 5K and 6C).

In Fig. 6D,  $d_{AP}$  gradually decreased throughout the action potential before rapidly declining at the end of the EAD.  $f_{AP}$  decreased monotonously to a minimum of 0.023 at 1157 msec and increased slightly at the end of the EAD.  $f_{AP_V}$  and  $f_{AP_{Ca}}$  also decreased during the action potential before increasing slightly at the end of the EAD (Figs. 6D and F). Again,  $I_{Ca,L}$  channels mediated a measurable inward current at  $T_{min}$  in spite of the small  $f_{AP}$  (Fig. 5F). This current was eventually eliminated by deactivation induced by delayed activation of  $I_{K1}$  channels ~300 msec after  $T_{min}$  (Figs. 5F, 5L and 6D).

Taken together, these results indicate that the common mechanism underlying these two types of EAD is the failure of complete deactivation of  $I_{Ca,L}$  channels and the resultant sustained inward current at the end of phase 2 repolarization.

## Discussion

### Inward currents induce early afterdepolarizations when delayed rectifier K<sup>+</sup> currents are blocked

E4031 and 293B evoked EADs when applied in combination to isolated guinea-pig ventricular myocytes (Fig. 1). When both I<sub>Kr</sub> and I<sub>Ks</sub> channels were completely blocked, EADs were not clearly separated from the preceding action potentials. This type of EADs would have the same pathophysiological effects on myocardial electrical activity as the prototypical phase 2 EADs such as conduction block and “prolonged repolarization-dependent reexcitation” (Brugada & Wellens, 1985).

A selective I<sub>Ca,L</sub> blocker nifedipine more potently shortened action potentials with EADs than those without EADs (Fig. 2). Thus, an I<sub>Ca,L</sub> current is critically involved in EADs caused by suppression of I<sub>Kr</sub> and I<sub>Ks</sub> currents (Marbán et al., 1986; Zeng & Rudy, 1995; Anderson et al., 1998). The Na-Ca exchanger blocker SEA0400 had a lesser inhibitory effect on EADs than nifedipine under this condition.

### Mechanism underlying early afterdepolarizations

January and Riddle (1989) analyzed EADs induced by the I<sub>Ca,L</sub> channel agonist BayK8644 in sheep Purkinje fibers and concluded that I<sub>Ca,L</sub> channels recovered before EADs and generated EADs. The EADs they found took off at ~-30 mV and had an amplitude of up to ~40 mV. They also showed that the amplitude of EADs was inversely correlated with the take-off potential of EADs, indicating that the recovery of I<sub>Ca,L</sub> channels before EADs is strongly dependent on the take-off potential. When I<sub>Kr</sub> and I<sub>Ks</sub> channels were suppressed, EADs took off at more depolarized potentials (~-10-0 mV) and had a much smaller amplitude (<15 mV) than January and Riddle (1989) found (Fig. 1). Under this condition, I<sub>Ca,L</sub> channels recovered only modestly if any before EADs took off (Figs. 6C and 6D).

A theoretical study indicated that the recovery and reactivation of I<sub>Ca,L</sub> channels also caused EADs when K<sup>+</sup> currents were suppressed (Zeng & Rudy, 1995). In this model,  $f_{AP\_Ca}$  rapidly reaches a minimum of ~0.1 during the initial ~10 msec and then increases up to ~0.5 before EADs take off. Thus, Ca<sup>2+</sup>-dependent inactivation proceeds very rapidly and reverses substantially. The authors reasoned that when action potentials were longer, I<sub>Ca,L</sub> channels recovered further from Ca<sup>2+</sup>-dependent inactivation during action potentials and thereby induced EADs. However,  $f_{AP\_Ca}$  in the model was a pure function of intracellular Ca<sup>2+</sup> concentration and thus mirrors a simulated intracellular Ca<sup>2+</sup> transient (Luo & Rudy, 1994). These predictions differ from our experimental results (Figs. 4C, 4D, 6C and 6D) where I<sub>Ca,L</sub> channels did not recover during action

potentials either as promptly nor as substantially as suggested by the model.

We found that in action potentials the decay of  $I_{Ca,L}$  currents after  $T_{min}$  resulted from deactivation, in which the regenerative activation of  $I_{K1}$  currents soon after  $T_{min}$  played a particularly important role (Figs. 3K, 4C and 4D) (Luo & Rudy, 1994; Linz and Myer, 1998a and 2000). When  $I_{Kr}$  and  $I_{Ks}$  channels were blocked, activation of  $I_{K1}$  channels and complete deactivation of  $I_{Ca,L}$  channels did not occur so soon after  $T_{min}$  (Figs. 3F, 3L and 4D). We speculate that this more sustained  $I_{Ca,L}$  current after  $T_{min}$  contributes to the genesis of EADs by block of  $I_{Kr}$  and  $I_{Ks}$  channels (Fig. 3F).

We analyzed two types of action potentials with EADs (Figs. 5A and B). In both cases, there were sustained  $I_{Ca,L}$  currents during EADs until they were completely deactivated by  $I_{K1}$  currents at the end of EADs (Figs. 5E, 5F, 5K, 5L, 6C and 6D). These results suggest that the essential mechanism underlying EADs is the failure of complete deactivation of  $I_{Ca,L}$  channels when  $I_{Kr}$  and  $I_{Ks}$  channels are suppressed. Depending on the extent of repolarization before EADs take off,  $I_{Ca,L}$  channels can recover from  $Ca^{2+}$ -dependent inactivation and subsequent regenerative activation of  $I_{Ca,L}$  channels would create the upstroke of EADs (Fig. 5E and 6C). However, this phenomenon was modest if any and did not seem to be essential for EADs when  $I_{Kr}$  and  $I_{Ks}$  currents were suppressed. Submicromolar nifedipine effectively suppressed EADs (Fig. 2) probably because it partially reduced  $I_{Ca,L}$  currents at the end of the phase 2 repolarization, allowed activation of  $I_{K1}$  channels and the complete deactivation of  $I_{Ca,L}$  channels.

$Ca^{2+}$ -induced facilitation of  $I_{Ca,L}$  channels may be involved in the genesis of EADs (Wu et al., 1999). The prolonged  $Ca^{2+}$  transient associated with prolonged action potentials may increase  $I_{Ca,L}$  currents by activating the calmodulin-dependent kinase. However, we did not see clear  $Ca^{2+}$ -induced facilitation when action potentials with EADs were applied to myocytes, nor did we find larger  $I_{Ca,L}$  currents in longer action potentials (Figs. 3E, 3F, 5E and 5F).

### **Clinical implications**

That nifedipine more potently shortened action potentials with EADs than without EADs in clinical blood concentrations ( $<1 \mu\text{M}$ ) (Fig. 2) indicates that nifedipine may not only suppress the trigger of the arrhythmias but also reduce the dispersion of refractoriness in LQT patients. Verapamil, a phenylalkylamine  $Ca^{2+}$  channel blocker, has been reported to be effective in suppressing epinephrine-induced EADs in familial LQT patients (Shimizu et al., 1995). Its mode of action may be the same as that shown for nifedipine in this study.

$\beta$ -Blocking agents are currently the major therapy for familial LQT patients when the genotype cannot be identified (Schwartz, 2005). This probably indicates that

$\beta$ -adrenergic stimulation increases  $I_{Ca,L}$  currents and the incidence of EADs. Because nifedipine and  $\beta$ -blocking agents are safely used in combination for many cardiovascular diseases (Hoffman, 2006; Michel, 2006), nifedipine (and probably also other dihydropyridines) can be a drug of choice for treatment of LQT patients with reduced delayed rectifier  $K^+$  currents.

### **Limitation of present study**

In ideal conditions of action potential clamp experiments each action potential stimulus should be derived from an action potential recorded in the same myocyte. To measure action potentials and  $f_{AP}$  in the same myocyte, it is necessary to automatically and promptly determine at which timing and potential action potentials should be interrupted to adequately assess  $f_{AP}$  within a span of a single patch-clamp experiment. However, this is usually difficult and requires fine manual adjustment especially in action potentials associated with EADs in which membrane potential changed slowly or passed the same value more than once. Thus, we analyzed the averages of the kinetics of  $I_{Ca,L}$  channels in exemplar action potentials and compared them with averaged channel currents in the exemplar action potentials as done by Linz & Myer (1998a).

We included 100  $\mu$ M EGTA in the pipette solution which would have modified the amplitude and kinetics of  $I_{Ca,L}$  currents. However, it should be noted that the peak  $I_{Ca,L}$  current density measured in this study was comparable with that measured without  $Ca^{2+}$  buffers (Doerr et al. 1990; Linz & Meyer, 1998a & 2000) but much smaller than that measured with strong  $Ca^{2+}$  buffers in pipette solutions (Arreola et al. 1991; Grantham & Cannell, 1996). We assessed  $f_{AP_V}$  by using  $Ba^{2+}$  as a permeant. However,  $Ba^{2+}$ -mediated  $I_{Ca,L}$  currents inactivate slightly faster and to a larger extent than  $Na^+$ -mediated ones in a range of action potentials (Findlay, 2002). Thus, we might have overestimated  $f_{AP_V}$ .

$Cd^{2+}$  used to block  $I_{Ca,L}$  currents modulate  $I_{Kr}$  and  $I_{Ks}$  currents in a voltage-dependent manner (Daleau et al., 1997). Thus,  $I_{Kr}$  and  $I_{Ks}$  currents measured in the presence of  $Cd^{2+}$  might have been over- or under-estimated by up to 30% depending on the membrane potential. The effect of  $Cd^{2+}$  on these  $K^+$  currents also might have caused an error in the measurement of  $f_{AP}$ . However,  $f_{AP}$  assessed when intra- and extra-cellular  $K^+$  was completely replaced with  $Cs^+$  and tetraethyl ammonium to block all  $K^+$  currents was not significantly different from that shown in Figs. 4 and 6.  $Cd^{2+}$  and  $Ba^{2+}$  also block  $I_{Na-Ca}$  currents (Blaustein and Lederer, 1999). However, isolated  $I_{Ca,L}$  and  $I_{K1}$  currents were not apparently contaminated with  $I_{Na-Ca}$  currents which are inward and as large as peak  $I_{Ca,L}$  currents near the end of action potentials (Figs. 3 and 5) (Armoundas et al., 2003).

During records, channel currents ran down. In experiments shown in Figs.3 and 5,

$\text{Cd}^{2+}$  plus nifedipine, E4031, 293B, and  $\text{Ba}^{2+}$  were respectively applied at  $85 \pm 3$ ,  $162 \pm 6$ ,  $256 \pm 9$  and  $341 \pm 14$  sec after formation of the whole-cell configuration. At these timings,  $I_{\text{Ca,L}}$ ,  $I_{\text{Kr}}$ ,  $I_{\text{Ks}}$  and  $I_{\text{K1}}$  currents ran down to  $99.6 \pm 4.6$ ,  $94.8 \pm 14.8$ ,  $92.7 \pm 6.3$  and  $91.5 \pm 5.0$  %, respectively.

The 200 msec prepulse to -40 mV might have affected the measurement of membrane currents,  $d_{\infty}$  and  $f_{AP}$ . Thus, we measured a total membrane current and  $f_{AP}$  in action potentials preceded by a 10 msec prepulse to -40 mV. The measured total membrane currents were not significantly different from those shown in Figs. 3 and 5.  $f_{AP}$  measured with a 10 msec prepulse was slightly but significantly higher than that measured with a 200 msec prepulse throughout an action potential. However,  $T_{min}$  was the same irrespective of the prepulse durations. Finally,  $V_{0.5}$  and  $k$  determining  $d_{\infty}$  (Eq. 2) was measured in rectangular voltage pulses preceded by a 10 or 200 msec prepulse to -40 mV. They were not significantly affected by the prepulse durations.

## References

- Alseikhan B.A., DeMaria C.D., Colecraft H.M., Yue D.T. (2002) Engineered calmodulins reveal the unexpected eminence of  $\text{Ca}^{2+}$  channel inactivation in controlling heart excitation, *PNAS* 99, 17185-17190
- Anderson M.E., Braun A.P., Wu Y., Lu T., Wu Y., Schulman H., Sung R.J. (1998) KN-93, an inhibitor of multifunctional  $\text{Ca}^{++}$ /calmodulin-dependent protein kinase, decreases early afterdepolarizations in rabbit heart, *J Pharmacol Exp Ther* 287, 996-1006
- Antzelevitch C., Shimizu W. (2002) Cellular mechanisms underlying the long QT syndrome, *Curr Opin Cardiology* 17, 43-51
- Armoundas, A.A., Hobai, I.A., Tomaselli, G.F., Winslow, R.L., O'Rourke, B. (2003) Role of sodium-calcium exchanger in modulating the action potential of ventricular myocytes from normal and failing hearts, *Circ Res* 93: 46-53
- Arreola J., Dirksen R.T., Shieh R.-C., Williford D.J., Sheu S. (1991)  $\text{Ca}^{2+}$  currents and  $\text{Ca}^{2+}$  transients under action potential clamp in guinea pig ventricular myocytes, *Am J Physiol* 261, C393-C397
- Birinyi P., Aesai K., Bányász T., Tóth A., Horváth B., Virág L., Szentandrassy N., Magyar J., Varró A., Fülöp F., Nánási P.P. (2005) Effects of SEA0400 and KB-R7943 on  $\text{Na}^+/\text{Ca}^{2+}$  exchange current and L-type  $\text{Ca}^{2+}$  current in canine ventricular cardiomyocytes, *Naunyn-Schmiedeberg's Arch Pharmacol* 372: 63-70
- Blaustein M.P., Lederer, W.J. (1999) Sodium/calcium exchange: its physiological implications, *Physiol Rev* 79: 763-854
- Bosch R.F., Gaspo R., Busch A.E., Lang H.J., Li G.-R., Nattel S. (1998) Effects of the chromanol 293B, a selective blocker of the slow, component of the delayed rectifier  $\text{K}^+$  current, on repolarization in human and guinea pig ventricular myocytes, *Cardiovasc Res* 38, 441-450
- Brugada P., Wellens H.J.J. (1985) Early afterdepolarizations: role in conduction block, "prolonged repolarization-dependent reexcitation," and tachyarrhythmia in the human heart, *Pace* 8: 889-896
- Cranefield P.F., Aronson R.S. (1988) The causes, characteristics, and consequences of early afterdepolarizations, In: Cranefield PF, Aronson RS (eds) *Cardiac arrhythmias: The role of triggered activity and other mechanisms*, Futura Pub. Co., New York, NY, USA, pp. 431-479
- Daleau, P., Khalifa, M., Turgeon, J. (1997) Effects of cadmium and nisoldipine on the delayed rectifier potassium current in guinea pig ventricular myocytes, *J Pharmacol Exp Ther* 281: 826-833

- Damiano B.P., Rose M.R. (1984) Effects of pacing on triggered activity induced by early afterdepolarizations, *Circulation* 5, 1013-1025
- Doerr T., Denger R., Doerr A., Trautwein W. (1990) Ionic currents contributing to the action potential in single ventricular myocytes of the guinea pig studied with action potential clamp, *Pflügers Arch* 416, 230-237
- Fabiato A. (1985) Simulated calcium current can both cause calcium loading in and trigger calcium release from the sarcoplasmic reticulum of a skinned canine cardiac Purkinje cell, *J Gen Physiol* 85, 291-320
- Findlay I. (2002) Voltage- and cation-dependent inactivation of L-type  $Ca^{2+}$  channel currents in guinea-pig ventricular myocytes, *J Physiol* 541, 731-740
- Grantham C.J., Cannell M.B. (1996)  $Ca^{2+}$  influx during the cardiac action potential in guinea pig ventricular myocytes, *Circ Res* 79, 194-200
- Hamill O.P., Marty A., Neher E., Sakmann B., Sigworth F.J. (1981) Improved patch-clamp techniques for high-resolution current recording from cells and cell-free membrane patches, *Pflügers Arch* 391, 85-100
- Hardley R.W., Lederer W.J. (1991)  $Ca^{2+}$  and voltage inactivate  $Ca^{2+}$  channels in guinea-pig ventricular myocytes through independent mechanisms, *J Physiol* 444, 257-268
- Hoffman B.B. (2006). Therapy of hypertension, In *The Pharmacological Basis of Therapeutics*, 11<sup>th</sup> edn, ed. Brunton LL, pp. 845-868. McGraw-Hill, New York, NY, USA.
- January C.T., Riddle J.M. (1989) Early afterdepolarizations: Mechanism of induction and block. A role for L-type  $Ca^{2+}$  current, *Circ Res* 64: 977-990
- Kass R.S., Sanguinetti M.C. (1984) Inactivation of calcium channel current in the calf cardiac Purkinje fiber. Evidence for voltage- and calcium-mediated mechanisms, *J Gen Physiol* 84, 705-726
- Keating M.T., Sanguinetti M.C. (2001) Molecular and cellular mechanisms of cardiac arrhythmias, *Cell* 104, 569-580
- Lee K.S., Marbán E., Tsien R.W. (1985) Inactivation of calcium channels in mammalian heart cells: Joint dependence on membrane potential and intracellular calcium, *J Physiol* 364, 395-411
- Linz K.W., Myer R. (1998a) Control of L-type calcium current during the action potential of guinea-pig ventricular myocytes, *J Physiol* 513, 425-442
- Linz K.W., Myer R. (1998b) The late component of L-type calcium current during guinea-pig cardiac action potentials and its contribution to contraction, *Pflügers Arch* 436, 679-688
- Linz K.W., Myer R. (2000) Profile and kinetics of L-type calcium current during the

- cardiac ventricular action potential compared in guinea-pigs, rats and rabbits, *Pflügers Arch* 439, 588-599
- Luo C.-H., Rudy Y. (1994) A dynamic model of the cardiac ventricular action potential. I. Simulations of ionic currents and concentration changes, *Circ Res* 74, 1071-1096
- Marbán E., Robinson S.W., Wier W.G. (1986) Mechanisms of arrhythmogenic delayed and early afterdepolarizations in ferret ventricular muscle, *J Clin Invest* 78, 1185-1192
- Matsuda T., Arakawa N., Takuma K., Kishida Y., Kawasaki Y., Sakaue M., Takahashi K., Takahashi T., Suzuki T., Ota T., Hamano-Takahashi A., Onishi M., Tanaka Y., Kameo K., Baba A. (2001) SEA0400, a novel and selective inhibitor of the  $\text{Na}^+$ - $\text{Ca}^{2+}$  exchanger, attenuates reperfusion injury in the in vitro and in vivo cerebral ischemic models, *J Pharmacol Exp Ther.* 298, 249-256
- McDonald T.F., Pelzer S., Trautwein W., Pelzer D.J. (1994) Regulation and modulation of calcium channels in cardiac, skeletal, and smooth muscle cells, *Physiol Rev* 74, 365-507
- Michel T. (2006). Treatment of myocardial ischemia, In *The Pharmacological Basis of Therapeutics*, 11<sup>th</sup> edn, ed. Brunton LL, pp. 823-844. McGraw-Hill, New York, NY, USA.
- Nagy Z.A., Virág L., Tóth A., Biliczki P., Acsai K., Bányász T., Nánási P., Papp J.G., Varró A. (2004) Selective inhibition of sodium-calcium exchanger by SEA-0400 decreases early and delayed afterpolarization in canine heart, *Br J Pharmacol* 143: 827-831
- Priori S.G., Corr P.B. (1990) Mechanisms underlying early and delayed afterpolarizations induced by catecholamines, *Am J Physiol* 27: H1796-H1805
- Sanguinetti M.C., Jurkiewicz N.K. (1990) Two components of cardiac delayed rectifier  $\text{K}^+$  current. Differential sensitivity to block by Class III antiarrhythmic agents, *J Gen Physiol* 96, 195-215
- Schwartz P.J. (2005). Management of long QT syndrome. *Nat Clin Pract Cardiovasc Med* 2, 346-351.
- Shimizu W., Ohe T., Kurita T., Kawade M., Arakaki Y., Aihara N., Kamakura S., Kamiya T., Shimomura K. (1995) Effects of verapamil and propranolol on early afterdepolarizations and ventricular arrhythmias induced by epinephrine in congenital long QT syndrome, *J Am Coll Cardiol* 26, 1299-1309
- Shirokov R., Levis R., Shirokova N., Ríos E. (1993)  $\text{Ca}^{2+}$ -dependent inactivation of cardiac L-type  $\text{Ca}^{2+}$  channels does not affect their voltage sensor, *J Gen Physiol* 102, 1005-1030

- Sicouri S., Quist M., Antzelevitch C. (1996) Evidence for the presence of M cells in the guinea pig ventricle, *J Cardiovasc Electrophysiol* 7, 503-511
- Splawski I., Timothy K.W., Sharpe L.M., Decher N., Kumar P., Bloise R., Napolitano C., Schwartz P.J., Joseph R.M., Condouris K., Tager-Flusberg H., Priori S.G., Sanguinetti M.C., Keating M.T. (2004)  $Ca_v1.2$  calcium channel dysfunction causes a multisystem disorder including arrhythmia and autism, *Cell* 119, 19-31
- Wu Y., MacMillan L.B., McNeill R.B., Colbran R.J., Anderson M.E. (1999) CaM kinase augments cardiac L-type  $Ca^{2+}$  current: a cellular mechanism for long Q-T arrhythmias, *Am J Physiol* 276, H2168-H2178
- Yamada M., Jahangir A., Hosoya Y., Inanobe A., Katada T., Kurachi Y. (1993)  $G_{K^*}$  and brain  $G_{\beta\gamma}$  activate muscarinic  $K^+$  channel through the same mechanism, *J Biol Chem* 268,24551-24554
- Zeng J., Rudy Y. (1995) Early afterdepolarizations in cardiac myocytes: Mechanism and rate dependence, *Biophys J* 68, 949-964

#### **Acknowledgements**

We are grateful to Dr. Ian Findlay (Centre National de la Recherche Scientifique UMR 6542, Faculté des Sciences, Université François Rabelais de Tours, France) for critical reading of this manuscript, and Ms. Reiko Sakai for secretarial assistance.

## Figure Legends

### Figure 1: Effects of E4031 and chromanol 293B on the action potentials of isolated guinea-pig ventricular myocytes

Isolated guinea-pig ventricular myocytes were paced at 0.33 Hz under the experimental conditions indicated with each trace. Figures A-D and E-H show representative traces recorded from two different myocytes. In each case, between 10-20 consecutively recorded action potentials in the steady-state are superimposed. In H, most of the action potentials were longer than the time span of the graph. 293B indicates chromanol 293B.

### Figure 2: The effect of nifedipine on action potentials recorded in the presence and absence of E4031 and chromanol 293B

A: Action potentials were recorded by pacing myocytes at 0.33 Hz. In the presence (below) and absence (above) of 10  $\mu$ M E4031 and 50  $\mu$ M 293B, first 10 and then 100 nM nifedipine was applied. B: APD<sub>90</sub> was measured in the presence of 10 or 100 nM nifedipine and expressed as a percentage of that recorded in the absence of nifedipine. Experiments were done in the absence (white bars) and presence (black bars) of 10  $\mu$ M E4031 and 50  $\mu$ M 293B. Error bars indicate SE of 5 observations. \*Statistically significant difference ( $p < 0.05$ ) as judged by Student's unpaired t-test.

### Figure 3: Total membrane, L-type Ca<sup>2+</sup> and K<sup>+</sup> currents flowing during action potential clamp

A, B: Action potentials used for action potential-clamp experiments with APD<sub>90</sub> of 396 and 606 msec, respectively. Action potential stimuli were applied to myocytes at 0.33 Hz. A represents control conditions, and the action potential in B was recorded in the presence of 10  $\mu$ M E4031 and 10  $\mu$ M 293B. C-L: time-dependent changes in the total myocyte current density ( $I_{total}$ ) (C, D) and the current density of  $I_{Ca,L}$  (E, F),  $I_{Kr}$  (G, H),  $I_{Ks}$  (I, J), and  $I_{K1}$  channels (K, L). In the experiments shown in the left column, Cd<sup>2+</sup> (100  $\mu$ M) plus nifedipine (10  $\mu$ M), E4031 (10  $\mu$ M), 293B (50  $\mu$ M), and Ba<sup>2+</sup> (2 mM) were sequentially added to myocytes in this order. First,  $I_{total}$  was measured in the absence of the drugs. Then,  $I_{Ca,L}$ ,  $I_{Kr}$ ,  $I_{Ks}$ , and  $I_{K1}$  were measured as a part of the membrane current density inhibited by Cd<sup>2+</sup> plus nifedipine, E4031, 293B, and Ba<sup>2+</sup>, respectively. In the experiments shown in the right column, Cd<sup>2+</sup> (100  $\mu$ M) plus nifedipine (10  $\mu$ M), E4031 (10  $\mu$ M), 293B (10  $\mu$ M), 293B (50  $\mu$ M), and Ba<sup>2+</sup> (2 mM) were sequentially added to myocytes in this order.  $I_{total}$ ,  $I_{Ca,L}$ ,  $I_{Kr}$ , and  $I_{K1}$  were measured as above. The black  $I_{Ks}$  trace in J was measured as a 293B (50  $\mu$ M)-sensitive difference

current density ( $I_{Ks-total}$ ). The gray  $I_{Ks}$  trace in J was measured as a difference between a current density before addition of 293B (50  $\mu$ M) (i.e. in the presence of 293B (10  $\mu$ M)) and that after addition of 293B (50  $\mu$ M) and represents  $I_{Ks}$  in the presence of 293B (10  $\mu$ M) ( $I_{Ks-10}$ ). The black  $I_{total}$  trace in D was measured as above while the gray was calculated as  $I_{total} - I_{Kr} - I_{Ks-total} + I_{Ks-10}$  and represents a total membrane current density in the presence of E4031 (10  $\mu$ M) and 293B (10  $\mu$ M). Note that  $I_{total}$  contains  $I_{Ca,L}$ ,  $I_{Kr}$ ,  $I_{Ks}$ ,  $I_{K1}$  and background currents. Each current trace is the mean of 5 stimuli. Horizontal lines indicate the zero potential (A, B) or current (C-L) level. Vertical dotted lines indicate the time of minimum  $I_{Ca,L}$  availability ( $T_{min}$ ) (left: 368 msec, right: 506 msec) (see Fig. 4).

#### Figure 4: The kinetics of L-type $Ca^{2+}$ channels during action potential clamp

A, B: The same representative action potentials shown in Fig. 3. C, D: Activation and inactivation of  $I_{Ca,L}$  channels in action potentials. Inactivation in action potentials was assessed with the gapped double pulse action potential clamp protocol. The action potential was interrupted when the membrane potential was +59, +54, +52, +50, +45, +40, +35, +30, +25, +20, +15, +10, 0, -10, -20, -30, -40, -50, -60, -70 mV and the resting membrane potential (-79 mV) in the left column; and +61, +53, +52, +50, +45, +40, +35, +30, +25, +20, +15, +10, 0, -10, -20, -30, -40, -50, -60, -70 mV and the resting membrane potential (-79 mV) in the right column. Continuous lines represent activation in action potentials ( $d_{AP}$ ). Symbols represent inactivation in action potentials in the presence of  $Ca^{2+}$  ( $\circ$ ,  $f_{AP}$ ) or  $Ba^{2+}$  ( $\triangle$ ,  $f_{AP_V}$ ). E, F: The  $Ca^{2+}$ -dependent component of inactivation in action potentials ( $\square$ ,  $f_{AP_{Ca}}$ ) estimated from  $f_{AP}$  and  $f_{AP_V}$  with Eq. 3. Symbols and bars represent mean and SE (n = 5 for each point). Vertical dotted lines indicate  $T_{min}$ .

#### Figure 5: L-type $Ca^{2+}$ and $K^+$ currents flowing during action potential stimuli showing early afterdepolarizations

A, B: Action potentials used for action potential-clamp experiments. The action potentials were recorded from two different myocytes paced at 0.33 Hz in the presence of 10  $\mu$ M E4031 and 20  $\mu$ M 293B (A) or 10  $\mu$ M E4031 and 50  $\mu$ M 293B (B). C-L: time-dependent changes in the total myocyte current density (C, D) and the current density of  $I_{Ca,L}$  (E, F),  $I_{Kr}$  (G, H),  $I_{Ks}$  (I, J), and  $I_{K1}$  channels (K, L). In the experiments shown in the left column,  $Cd^{2+}$  (100  $\mu$ M) plus nifedipine (10  $\mu$ M), E4031 (10  $\mu$ M), 293B (20  $\mu$ M), 293B (50  $\mu$ M), and  $Ba^{2+}$  (2 mM) were sequentially added to myocytes in this order. First,  $I_{total}$  was measured in the absence of the drugs (black trace in C). Then,  $I_{Ca,L}$ ,  $I_{Kr}$ , and  $I_{K1}$  were measured as a part of the membrane current density

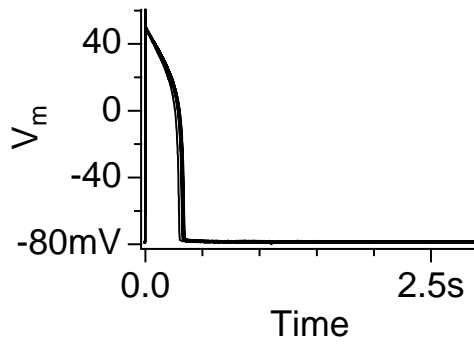
inhibited by  $\text{Cd}^{2+}$  plus nifedipine, E4031, and  $\text{Ba}^{2+}$ , respectively. The black  $I_{\text{Ks}}$  trace in I was measured as a 293B (50  $\mu\text{M}$ )-sensitive difference current density ( $I_{\text{Ks-total}}$ ). The gray  $I_{\text{Ks}}$  trace in I was measured as a difference between a current density before addition of 293B (50  $\mu\text{M}$ ) (i.e. in the presence of 293B (20  $\mu\text{M}$ )) and that after addition of 293B (50  $\mu\text{M}$ ) and represents  $I_{\text{Ks}}$  in the presence of 293B (20  $\mu\text{M}$ ) ( $I_{\text{Ks-20}}$ ). The grey  $I_{\text{total}}$  trace in C was calculated as  $I_{\text{total}} - I_{\text{Kr}} - I_{\text{Ks-total}} + I_{\text{Ks-20}}$  and represents a total membrane current density in the presence of E4031 (10  $\mu\text{M}$ ) and 293B (20  $\mu\text{M}$ ). In the experiments shown in the right column,  $\text{Cd}^{2+}$  (100  $\mu\text{M}$ ) plus nifedipine (10  $\mu\text{M}$ ), E4031 (10  $\mu\text{M}$ ), 293B (50  $\mu\text{M}$ ), and  $\text{Ba}^{2+}$  (2 mM) were sequentially added to myocytes in this order. First,  $I_{\text{total}}$  was measured in the absence of the drugs (black trace in D). Then,  $I_{\text{Ca,L}}$ ,  $I_{\text{Kr}}$ ,  $I_{\text{Ks}}$ , and  $I_{\text{K1}}$  were measured as a part of the membrane current density inhibited by  $\text{Cd}^{2+}$  plus nifedipine, E4031, 293B, and  $\text{Ba}^{2+}$ , respectively. The gray  $I_{\text{total}}$  trace in D was calculated as  $I_{\text{total}} - I_{\text{Kr}} - I_{\text{Ks}}$  and represents a total membrane current density in the presence of E4031 (10  $\mu\text{M}$ ) and 293B (50  $\mu\text{M}$ ). Note that  $I_{\text{total}}$  contains  $I_{\text{Ca,L}}$ ,  $I_{\text{Kr}}$ ,  $I_{\text{Ks}}$ ,  $I_{\text{K1}}$  and background currents. Each current trace is the mean of 5 stimuli. The arrow in E indicates a notch in  $I_{\text{Ca,L}}$  currents observed on the upstroke of the EAD. The arrow head in K indicates partial activation of  $I_{\text{K1}}$  channels before the EAD took off. Vertical dotted lines indicate  $T_{\text{min}}$  (left: 933 msec, right: 1158 msec).

**Figure 6: The kinetics of L-type  $\text{Ca}^{2+}$  channels during action potential stimuli showing early afterdepolarizations**

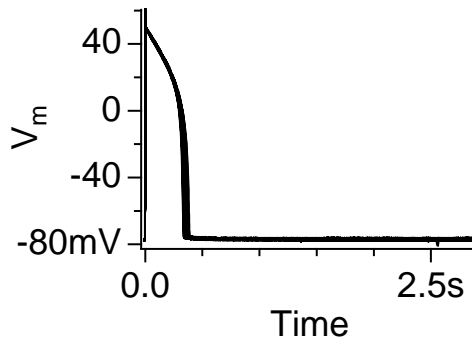
A, B: The same representative action potentials shown in Fig. 5. C, D: Activation and inactivation of  $I_{\text{Ca,L}}$  channels in action potentials. Inactivation in action potentials was assessed with the gapped double pulse action potential clamp protocol. The action potential was interrupted when the membrane potential was +61, +50, +45, +40, +35, +30, +25, +20, +15, +10, +4, -1, -6, -2, +1, 0, -4, -10, -20, -30, -40, -50, -60, -70 and the resting membrane potential (-77 mV); and +50, +49, +45, +40, +35, +30, +25, +20, +15, +10, +5, +2, -2, -10, -20, -30, -40, -50, -60, -70 and the resting membrane potential (-77 mV). Continuous lines indicate activation in action potentials ( $d_{\text{AP}}$ ). Symbols represent inactivation in action potentials in the presence of  $\text{Ca}^{2+}$  ( $\circ$ ,  $f_{\text{AP}}$ ) or  $\text{Ba}^{2+}$  ( $\triangle$ ,  $f_{\text{AP}_V}$ ). E, F: The  $\text{Ca}^{2+}$ -dependent component of inactivation in action potentials ( $\square$ ,  $f_{\text{AP}_{Ca}}$ ) was estimated from  $f_{\text{AP}}$  and  $f_{\text{AP}_V}$  with Eq. 3. Symbols and bars represent mean and SE (n = 5 for each point). Vertical dotted lines indicate  $T_{\text{min}}$ . \*Statistically significant difference (p < 0.05) as judged by Student's paired t-test.

Figure 1

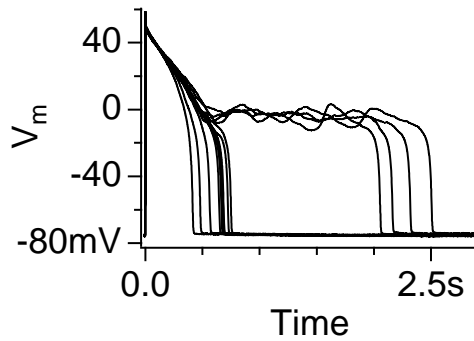
**A: Control**



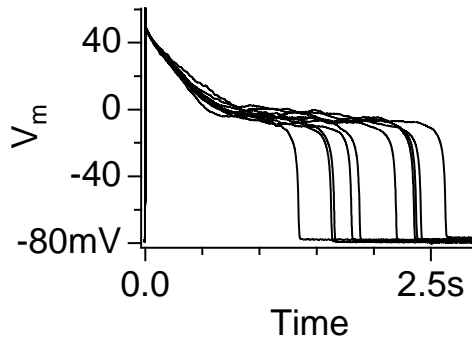
**B: E4031(10  $\mu$ M)**



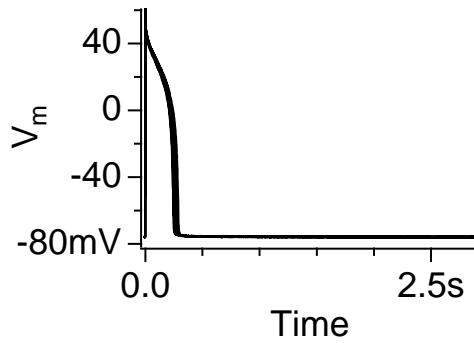
**C: E4031(10  $\mu$ M) + 293B(20  $\mu$ M)**



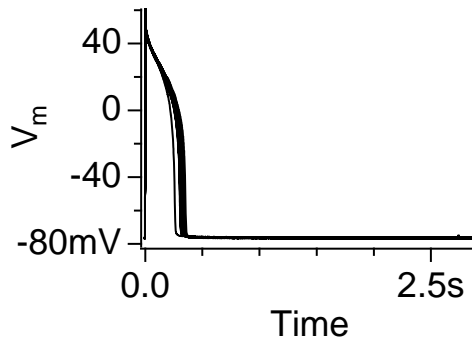
**D: E4031(10  $\mu$ M) + 293B(50  $\mu$ M)**



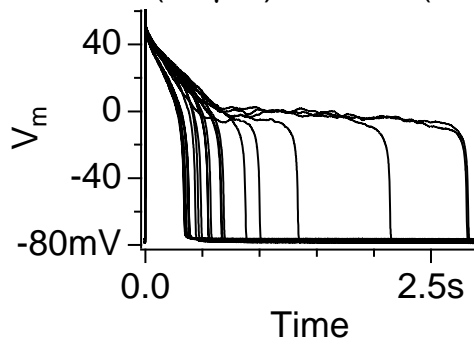
**E: Control**



**F: 293B(50  $\mu$ M)**



**G: 293B(50  $\mu$ M) + E4031(100 nM)**



**H: 293B(50  $\mu$ M) + E4031(1  $\mu$ M)**

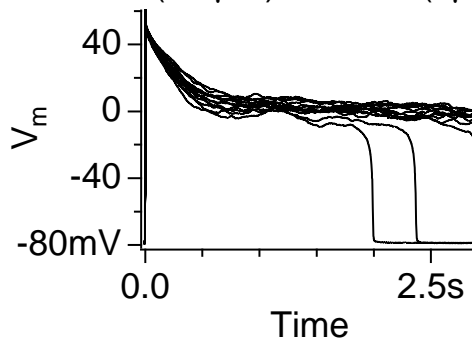


Figure 2

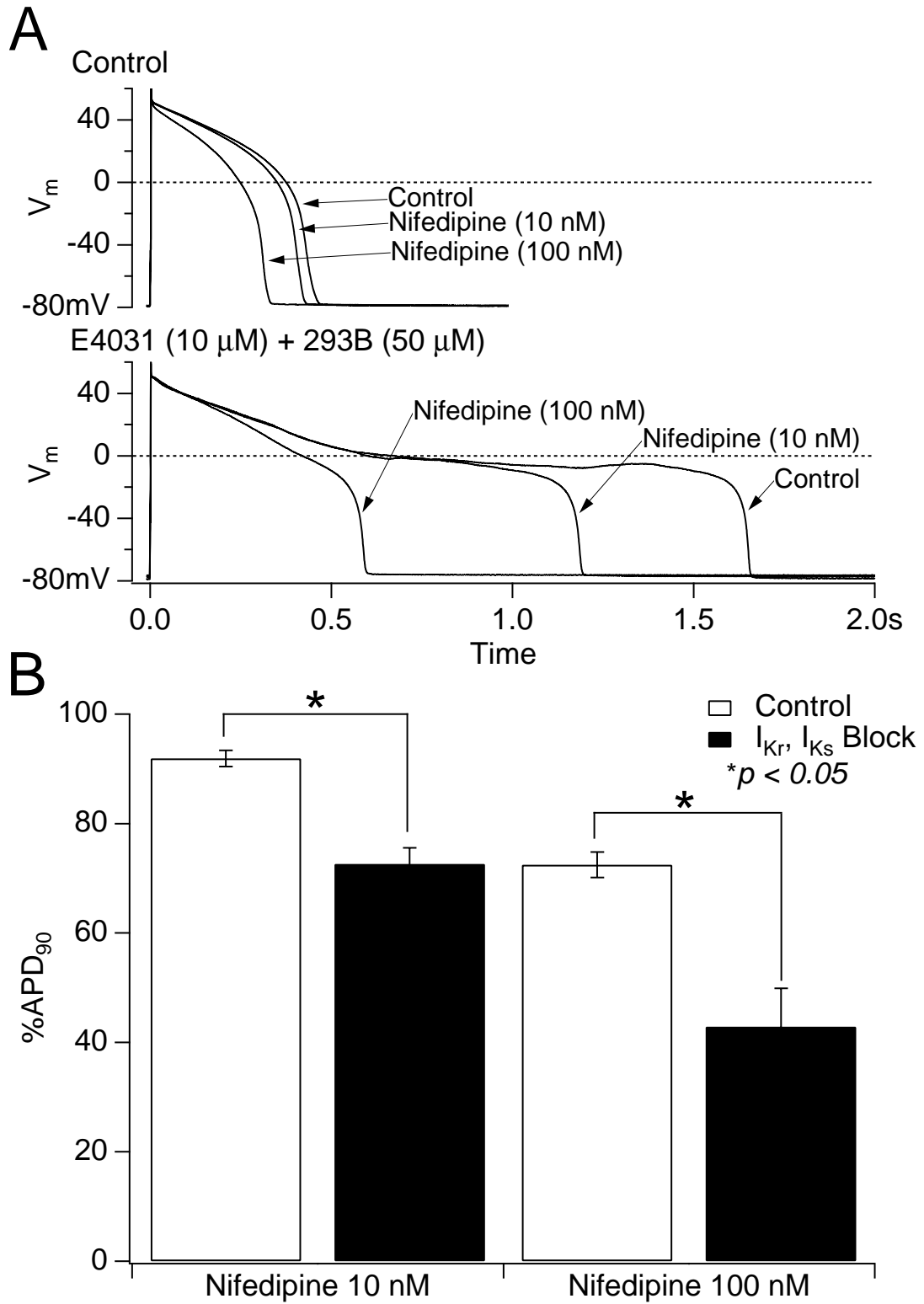


Figure 3

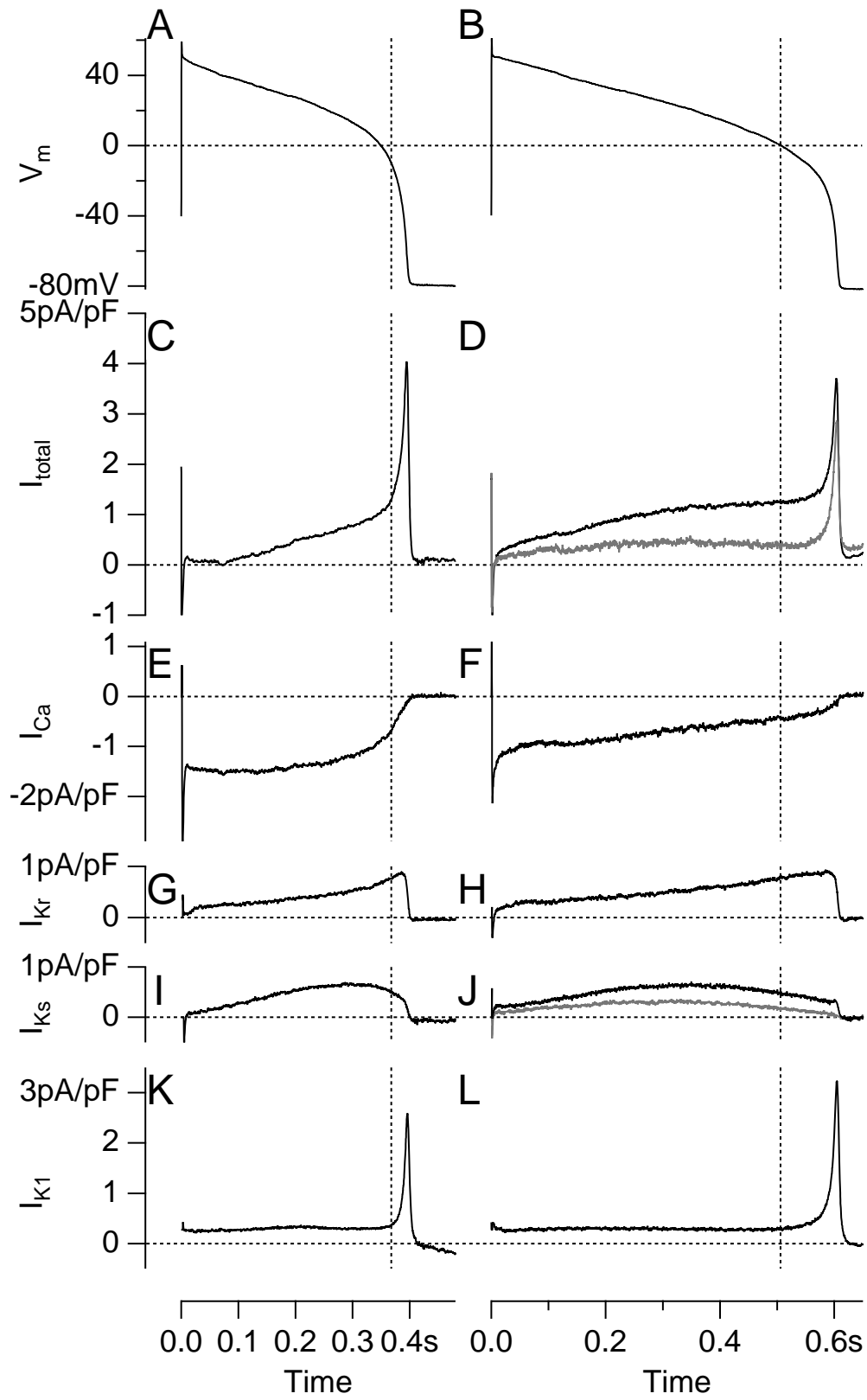


Figure 4

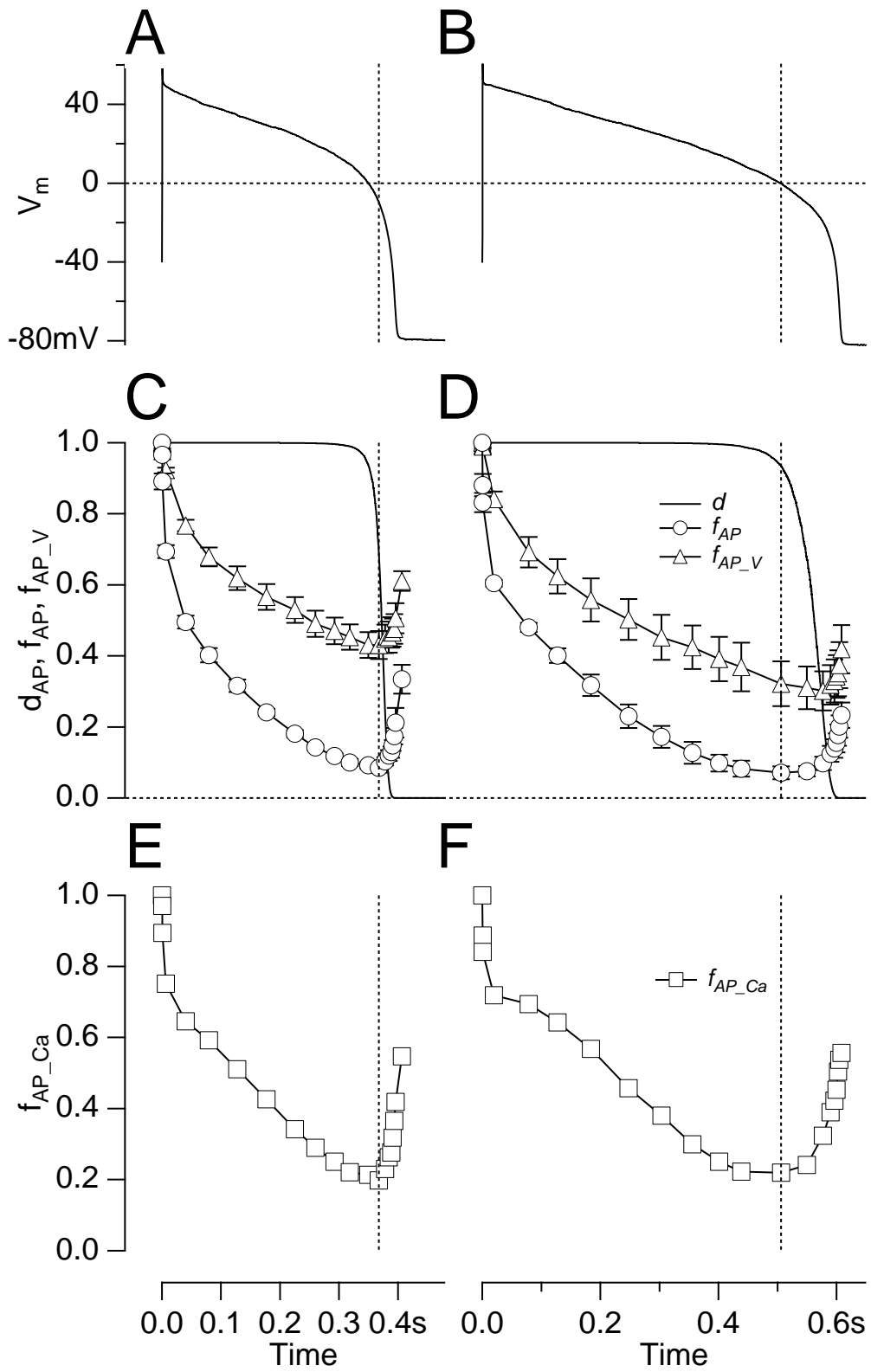


Figure 5

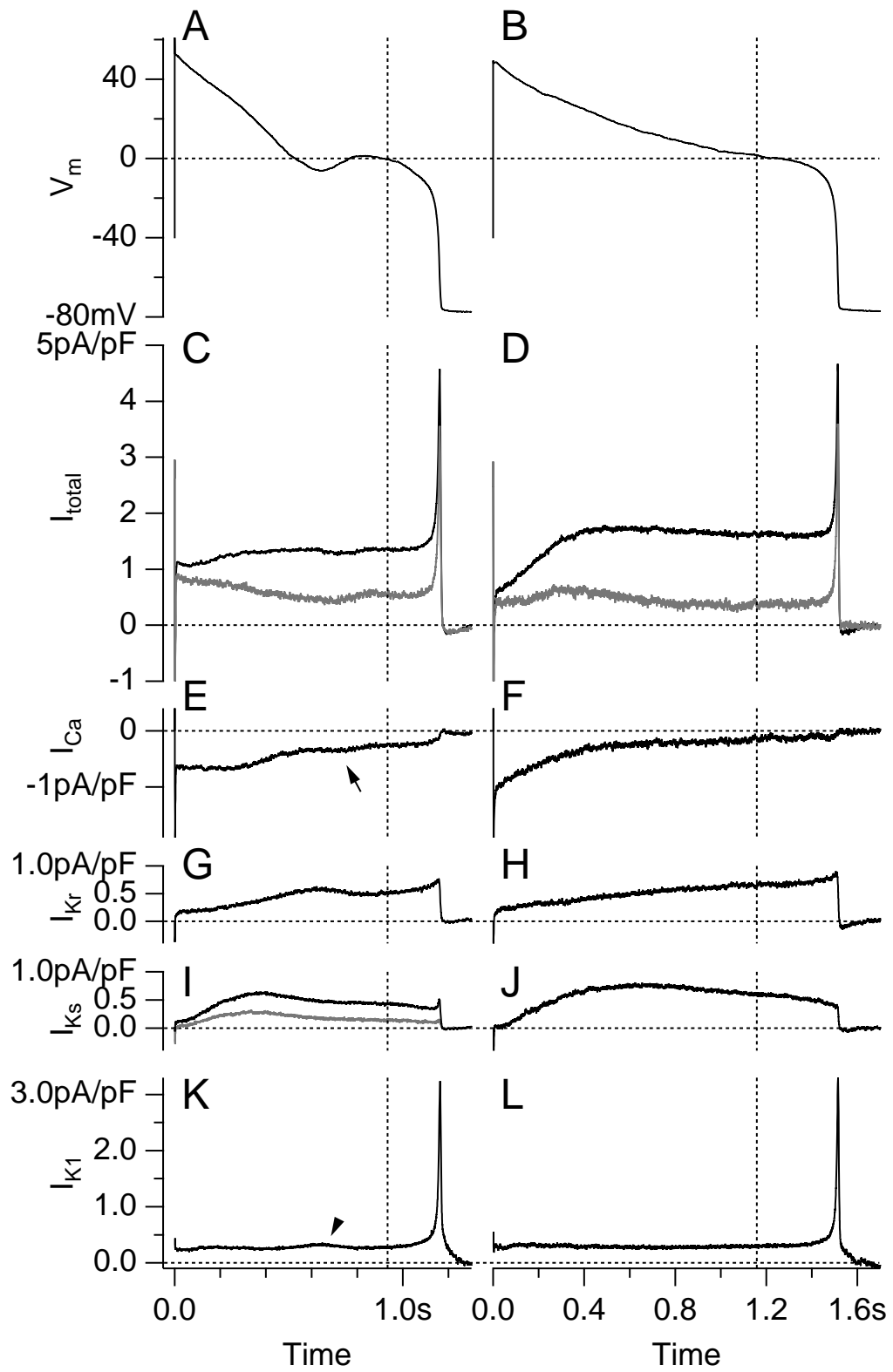


Figure 6

